*Journal of Thermal Analysis and Calorimetry, Vol. 72 (2003) 209–221*

# SURFACE ACIDITY OF SUPPORTED VANADIA CATALYSTS

*H. Zou*[1], *M. Li*[1], *J. Shen*[1,2*] *and A. Auroux*[2]

[1]Department of Chemistry, Nanjing University, Nanjing 210093, China
[2]Institut de Recherches sur la Catalyse, CNRS, 2 Avenue Einstein, 69626 Villeurbanne Cedex, France

## Abstract

The surface acidity of $SiO_2$, $\gamma$-$Al_2O_3$ and $TiO_2$ supported vanadia catalysts has been studied by the microcalorimetry and infrared spectroscopy using ammonia as the probe molecule. The acidity in terms of nature, number and strength was correlated with surface structures of vanadia species in the catalysts, characterized by X-ray diffraction and UV-Vis spectroscopy. It was found that the dispersion and surface structure of vanadia species depend on the nature of supports and loading and affect strongly the surface acidity. On $SiO_2$, vanadium species is usually in the form of polycrystalline $V_2O_5$ even for the catalyst with low loading (3%) and these $V_2O_5$ crystallites exhibit similar amount of Brönsted and Lewis acid sites. The 25%$V_2O_5$/$SiO_2$ catalyst possesses substantial amount of $V_2O_5$ crystallites on the surface with the initial heat of 105 kJ mol$^{-1}$ and coverage of about 600 μmol g$^{-1}$ for ammonia adsorption. Vanadia can be well dispersed on $\gamma$-$Al_2O_3$ and $T_iO_2$ to form isolated tetrahedral species and polymeric two-dimensional network. Addition of vanadia on $\gamma$-$Al_2O_3$ results in the change of acidity from that associated with $\gamma$-$Al_2O_3$ (mainly Lewis sites) to that associated with vanadia (mainly Brönsted sites) and leads to the decreased acid strength. The 3%$V_2O_5$/$T_iO_2$ catalyst may have the vanadia structure of incomplete polymeric two-dimensional network that possesses the Ti–O–V–OH groups at edges showing strong Brönsted acidity with the initial heat of about 140 kJ mol$^{-1}$ for ammonia adsorption. On the other hand, the 10%$V_2O_5$/$TiO_2$ catalyst may have well defined polymeric two-dimensional vanadia network, possessing V–O–V–OH groups that exhibit rather weak Brönsted acidity with the heat of 90 kJ mol$^{-1}$ for $NH_3$ adsorption. $V_2O_5$ crystallites are formed on the 25%$V_2O_5$/$TiO_2$ catalyst, which exhibit the acid properties similar to those for 25%$V_2O_5$ on $SiO_2$ and $\gamma$-$Al_2O_3$.

**Keywords:** infrared spectroscopy, microcalorimetry, supported vanadia catalysts, surface acidity

## Introduction

Supported vanadia catalysts have found wide applications. For example, they have been used for selective oxidation of *o*-xylene to phthalic anhydride [1, 2], ammoxidation of alkyl aromatics [3, 4], selective catalytic reduction of $NO_x$ with $NH_3$ [5], oxidation of $SO_2$ to $SO_3$ [5–7], oxidative dehydrogenation of alkanes to olefins [8], oxidation of butane and pentane to maleic anhydride [9–12] and selective oxidation of methanol to formaldehyde [13] or methyl formate [14].

* Author for correspondence: E-mail: jyshen@nju.edu.cn

*1388–6150/2003/ $ 20.00*
*Akadémiai Kiadó, Budapest*

Vanadia catalysts may exhibit different catalytic properties because of the metal oxide-support interactions that affect both redox properties and dispersity of the active phase. Numerous spectroscopic studies have been carried out to highlight the nature of the surface structures of vanadium species and their stability. These studies revealed the different forms of vanadia for different supports and loadings. When the loading is low (<5%), vanadia can be highly dispersed to form isolated tetrahedral vanadate species. With the increase of loading, vanadia species may form polymeric two-dimensional network in distorted tetrahedral and square-pyramidal coordination. Finally, at high loadings, three-dimensional $V_2O_5$ crystallites in octahedral coordination are formed [15–20].

The acidity of supported-vanadia has also been studied [21–24]. Unsupported $V_2O_5$ crystalline powders possess both surface Brönsted and Lewis acid sites [25]. The formation of the surface vanadia species on the oxide supports such as $\gamma$-$Al_2O_3$ and $TiO_2$ is accompanied by a decrease in the number of surface Lewis acid sites and an increase in the number of surface Brönsted acid sites [26, 27]. Turek and Wachs [24] suggested that at monolayer coverage, the fraction of surface metal oxide species possessing Brönsted acidity correspond to about 5–10% of the total number of surface sites and the surface Brönsted acid sites are probably located at the bridging M–O-support bonds. However, no direct spectroscopic evidence is currently available to support the assignment of location of the surface Brönsted acid sites.

The surface acidity and redox properties are the most important aspects of vanadia catalysts since they determine the catalytic behavior. These properties are apparently governed by the nature of support and the surface structure of vanadia species. Hence, a correlation of these properties with structure of supported vanadia is helpful for the catalyst design. The purpose of this paper is to provide a correlation between the surface acidity and the surface structure of vanadia species for the $SiO_2$, $\gamma$-$Al_2O_3$ and $TiO_2$ supported vanadia catalysts. Microcalorimetric adsorption of ammonia has been used to probe the surface acidity. This technique in combination with infrared spectroscopy has been proved to be powerful in elucidating the nature, number and strength of surface acid sites of solid catalysts [28]. In addition, X-ray diffraction (XRD) and UV-Visible spectroscopy (DRS) were used to characterize the surface structure of the catalysts.

## Experimental

*Catalyst preparation*

The supported-vanadia catalysts with different loadings of $V_2O_5$ (3, 10 and 25 wt%) were prepared by the incipient wetness impregnation method by using the solution containing $NH_4VO_3$ and $H_2C_2O_4 \cdot 2H_2O$ (mass ratio: 1/2). The supports used are $SiO_2$ (360 $m^2\ g^{-1}$), $\gamma$-$Al_2O_3$ (160 $m^2\ g^{-1}$) and $TiO_2$ (53 $m^2\ g^{-1}$). After the impregnation, the samples were dried at 393 K for 12 h and then calcined at 673 K for 6 h in air. A bulk $V_2O_5$ was also prepared as the reference by calcining $NH_4VO_3$ at 673 K for 4 h.

## Catalyst characterization

The X-ray diffraction was performed on a Riaku D/Max-RA X-ray diffractometer using the $CuK_\alpha$ X-ray source. The applied voltage and current were 40 kV and 80 mA, respectively. The scanning rate was 4 deg $min^{-1}$. DRS spectra were taken on a Shimadzu UV2100 UV-Vis Recording Spectrophotometer at room temperature. The spectra were recorded against a halon white reflectance standard in the range of 900–190 nm.

Microcalorimetric adsorption of $NH_3$ was carried out on a Tian–Calvet heat-flux apparatus. The microcalorimeter was connected to a gas-handling and volumetric adsorption system, equipped with a Baratron capacitance manometer for precision pressure measurement. The differential heat of adsorption *vs.* adsorbate coverage was obtained by measuring the heats evolved when doses of a gas (1–5 μmol) were admitted sequentially onto the catalyst until the surface was saturated by the adsorbate. Before microcalorimetric measurements, the samples were dried under vacuum at 573 K for 1 h, calcined in 500 Torr $O_2$ at 673 K for 2 h, and evacuated at 673 K for 2 h. Microcalorimetric adsorption of ammonia was performed at 423 K.

Infrared spectra were collected with an IFS66V Vacuum-type FT-IR Spectrophotometer. Each spectrum was recorded at 2 $cm^{-1}$ resolution with 32 co-added scans. Sample pellets were formed with a thickness of 20–30 mg $cm^{-2}$. The samples were loaded into a quartz cell equipped with $CaF_2$ windows. The treatment procedure of the samples for IR was the same as for microcalorimetric adsorption studies. Ammonia was dosed onto the sample at room temperature and held in the sample cell for 0.5 h before it was evacuated. Each reported spectrum was the difference between the spectrum of the clean sample and the spectrum after dosing ammonia.

## Results and discussion

### *$V_2O_5/SiO_2$*

Figure 1 shows the XRD patterns of the $V_2O_5/SiO_2$ catalysts with different loadings. Only a broad upheaval due to amorphous $SiO_2$ support was detected for the $3\%V_2O_5/SiO_2$ sample. The XRD peaks for $V_2O_5$ crystalline were not clearly seen for the $10\%V_2O_5/SiO_2$ catalyst. However, the $25\%V_2O_5/SiO_2$ catalyst exhibited XRD diffraction peaks around 26, 20.2 and 21.5° owing to the $V_2O_5$ crystallites on the $SiO_2$ support. X-ray line broadening analysis using the Scherrer equation shows that the $V_2O_5$ crystallites on $SiO_2$ may have diameters of 30–40 nm. Khodakov *et al*. [29] pointed out that smaller $V_2O_5$ crystallites might be present for the samples with lower $VO_x$ loadings, which could not be detected by the diffraction method because of their low concentration, poor crystallinity, or small numbers of unit cells.

UV-vis absorption spectra reflect the electronic structure of valence bands in solids, but the broad nature of charge transfer features in the spectra of metal oxides makes it difficult to define the position of these bands from the energy at maximum absorption. Absorption edge energies provide a more convenient description of the electronic properties of solids. The absorption edge in a DRS spectrum can be deter-

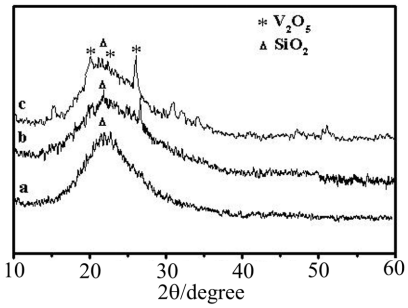


**Fig. 1** X-ray diffraction patterns for $V_2O_5/SiO_2$ samples with the $V_2O_5$ loading of a – 3%, b – 10% and c – 25%

mined using the Tauc's law, an expression describing the metal-edge region in amorphous and crystalline semiconductors with indirect band gap transitions [30]. The energy at the absorption edge has recently been used to characterize the size of $MoO_x$ [31], $WO_x$ [32], and $VO_x$ [33] domains in catalytic solids. Higher energy of charge transfer transition was observed for the smaller domain size of semiconductors [31, 34–35]. The bands observed in the range 2–4 eV arise from low energy charge transfer from $O^{2-}$ to $V^{5+}$ [36–39]. For $V^{4+}$ species, such transitions occur at higher energies (4.5–5 eV). The DRS spectra of the $V_2O_5/SiO_2$ catalysts studied in this work are shown in Fig. 2. The three $V_2O_5/SiO_2$ samples with different loadings had almost the same edge energies, close to that of bulk $V_2O_5$, indicating the similar crystalline nature of the surface $V_2O_5$ for these catalysts. The $25\%V_2O_5/SiO_2$ sample had the absorption edge energy even closer to that of bulk $V_2O_5$ (~2.12 eV), demonstrating that this sample had the surface $V_2O_5$ crystallites similar to the bulk.

In Fig. 3 are shown the differential heats of adsorption *vs.* coverage of ammonia on $SiO_2$ and $V_2O_5/SiO_2$ samples. The initial heat and coverage for ammonia adsorption on $SiO_2$ were quite low (35 kJ $mol^{-1}$ and 150 μmol $g^{-1}$), because of the hydrogen bonding of ammonia to the hydroxyl groups of $SiO_2$ surface. The addition of $3\%V_2O_5$ increased the initial heat of ammonia adsorption to 41 kJ $\mu mol^{-1}$ and the saturation ammonia coverage to 200 mol $g^{-1}$. The initial heat and coverage were substantially in-

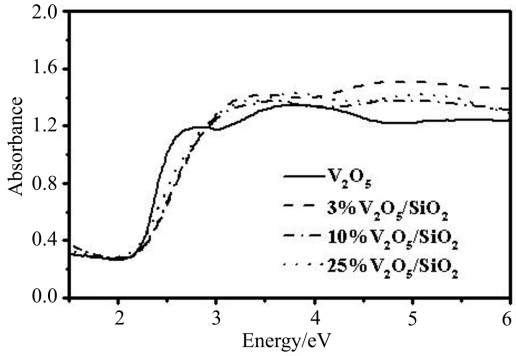


**Fig. 2** DRS spectra for $V_2O_5/SiO_2$ catalysts

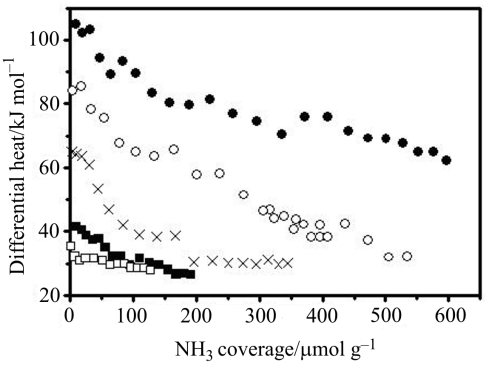


**Fig. 3** Differential heat *vs.* adsorbated coverage for adsorption of $NH_3$ at 423 K □ – $SiO_2$, ■ – $V_2O_5/SiO_2$, ○ – 10%$V_2O_5/SiO_2$, ● – 25% $V_2O_5/SiO_2$, × – 10%$V_2O_5/SiO_2$ treated in $H_2$ at 640 K

creased to 83 kJ μmol$^{-1}$ and 550 μmol g$^{-1}$ for ammonia adsorption when the loading of $V_2O_5$ was increased to 10%. The initial heat and ammonia coverage were further increased to 105 kJ mol$^{-1}$ and 600 μmol g$^{-1}$, respectively, for the 25%$V_2O_5/SiO_2$ sample. The reduction of the $V_2O_5/SiO_2$ samples in $H_2$ at 640 K significantly decreased the surface acidity. For example, the reduction of the 10%$V_2O_5/SiO_2$ samples led to the decrease of the initial heat to 65 kJ mol$^{-1}$ and ammonia coverage to 350 μmol/g, respectively.

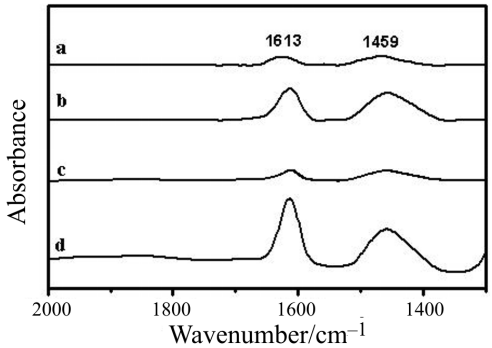


**Fig. 4** FT-IR spectra collected after ammonia adsorption at room temperature on $V_2O_5/SiO_2$ catalysts with the $V_2O_5$ loading of a – 3%, b – 10%, c – 25%, d – 10% $V_2O_5/SiO_2$ treated in $H_2$ at 640 K

Figure 4 shows the IR spectra collected after exposure of the $V_2O_5/SiO_2$ samples to ammonia at room temperature. The band around 1613 cm$^{-1}$ can be assigned to asymmetric deformation vibration of $NH_3$ coordinated to vanadium cations, representing the Lewis acid sites. The band at 1459 cm$^{-1}$ is attributed to $NH_4^+$ species formed by the interaction of $NH^3$ with surface Brönsted acid sites. The intensities of

these two bands increased with the increase of $V_2O_5$ loading. The intensities of these two bands were decreased simultaneously for the 10%$V_2O_5$/$SiO_2$ sample after reduction. These results indicate that both Lewis and Brönsted acid sites were present substantially on the surface of $V_2O_5$/$SiO_2$ catalysts and the nature of these acidities were not altered upon the reduction of vanadium species.

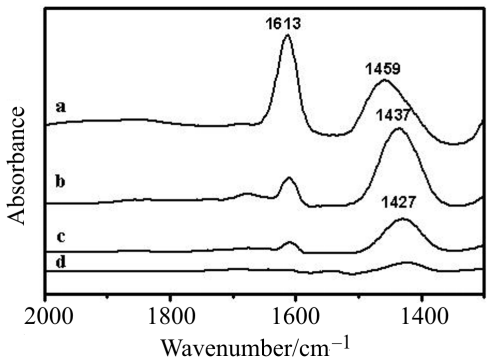


**Fig. 5** FT-IR spectra collected after ammonia adsorption a – at room temperature on 25%$V_2O_5$/$SiO_2$ catalysts, followed by evacuation at b – 298 K, c – 328 K and d – 373 K

In order to compare the relative strength of Lewis and Brönsted acidities on the $V_2O_5$/$SiO_2$ catalysts, we evacuated the 25%$V_2O_5$/$SiO_2$ samples at different temperatures after the ammonia adsorption. Figure 5 shows clearly that the intensity of the band around 1613 cm$^{-1}$ for Lewis acidity decreased faster than the intensity of the band around 1450 cm$^{-1}$ for Brönsted acidity. This revealed that the Brönsted acidity was stronger than Lewis acidity for the $V_2O_5$/$SiO_2$ samples.

*$V_2O_5$/γ-$Al_2O_3$*

Figure 6 shows the XRD patterns for the $V_2O_5$/γ-$Al_2O_3$ catalysts. Only XRD peaks for γ-$Al_2O_3$ were detected for the 3%$V_2O_5$/γ-$Al_2O_3$ and 10%$V_2O_5$/γ-$Al_2O_3$ samples. For the 25%$V_2O_5$/γ-$Al_2O_3$ sample, the peaks for $V_2O_5$ crystallites were clearly seen besides those for γ-$Al_2O_3$.

UV-Vis absorption spectra for the $V_2O_5$/γ-$Al_2O_3$ samples are shown in Fig. 7. The absorption edge energy for the 3%$V_2O_5$/γ-$Al_2O_3$ sample appears around 3.97 eV, which can be attributed to the monomeric vanadia species on the γ-$Al_2O_3$ support [34]. With the increase of $V_2O_5$ loading, the absorption edge energy decreased substantially and moved toward that of bulk $V_2O_5$. In fact, the 10%$V_2O_5$/γ-$Al_2O_3$ and 25%$V_2O_5$/γ-$Al_2O_3$ samples exhibited the similar absorption edge energies around 2.85 eV, indicating some similarity for the surface vanadia species in these two samples. According to the XRD and DRS results, it may be concluded that the isolated tetrahedral vanadia species might be formed on the surface of the 3%$V_2O_5$/γ-$Al_2O_3$ sample while the polymeric two-dimensional network of vanadia species might be formed on the surface of the 10%$V_2O_5$/γ-$Al_2O_3$ sample.

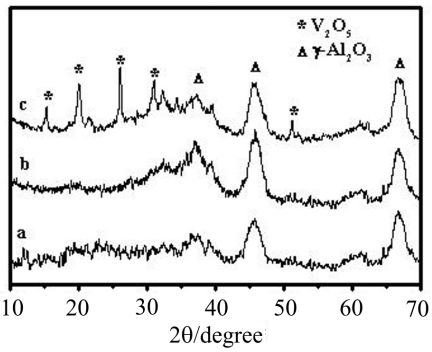


**Fig. 6** X-ray diffraction patterns for $V_2O_5/\gamma$-$Al_2O_3$ samples with the $V_2O_5$ loading of a – 3%, b – 10% and c – 25%

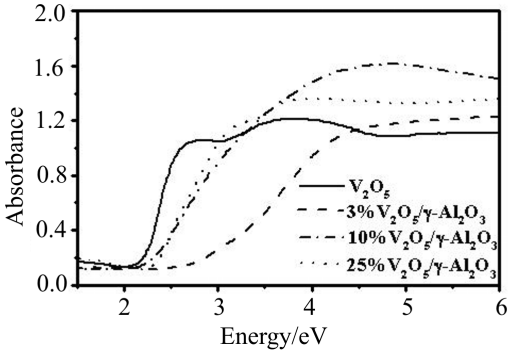


**Fig. 7** DRS spectra for $V_2O_5/\gamma$-$Al_2O_3$ catalysts

Finally, when the $V_2O_5$ loading reached 25%, crystalline $V_2O_5$ were formed besides the polymeric two-dimensional vanadia network species.

Different forms of vanadia species on the $\gamma$-$Al_2O_3$ may result in different surface acidities for the samples. Figure 8 shows the results for the microcalorimetric adsorption of ammonia on these samples as well as on $\gamma$-$Al_2O_3$. The initial heat and coverage for ammonia adsorption on the $\gamma$-$Al_2O_3$ support used were measured to be about 140 kJ $mol^{-1}$ and 420 μmol $g^{-1}$, respectively. The addition of $V_2O_5$ seemed to decrease the initial heat of ammonia adsorption. For example, the initial heat and coverage were found to be about 135 kJ $mol^{-1}$ and 280 μmol $g^{-1}$, respectively, for the 3%$V_2O_5/\gamma$-$Al_2O_3$ sample. This implies that added $V_2O_5$ covered some strong acid sites of the $\gamma$-$Al_2O_3$ support. The initial heats were further decreased to 125 and 120 kJ $mol^{-1}$, when the $V_2O_5$ loading was increased to 10 and 25%, respectively. However, the uptakes of ammonia for the 10%$V_2O_5/\gamma$-$Al_2O_3$ and 25%$V_2O_5/\gamma$-$Al_2O_3$ samples were increased to 500 μmol $g^{-1}$, owing to the adsorption of ammonia on vanadium sites. In addition, the heat was higher on the 25%$V_2O_5/\gamma$-$Al_2O_3$ than on the other samples for the ammonia coverage higher than 150 μmol $g^{-1}$. This increased heat can be

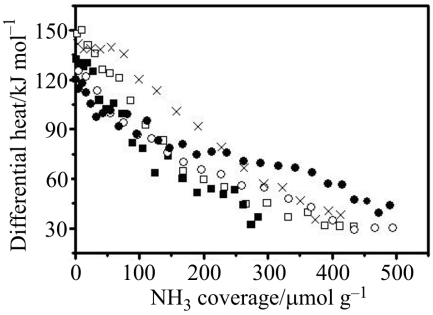


**Fig. 8** Differential heat *vs*. adsorbate coverage for adsorption of $NH_3$ at 423 K □ – γ-$Al_2O_3$, ■ – 3% $V_2O_5$/γ-$Al_2O_3$, ○ – 10% $V_2O_5$/γ-$Al_2O_3$, ● – 25% $V_2O_5$/γ-$Al_2O_3$ and × – 10% $V_2O_5$/γ-$Al_2O_3$ treated in $H_2$ at 640 K

attributed to the ammonia adsorption on crystalline $V_2O_5$ on the γ-$Al_2O_3$ support. After the reduction in $H_2$, the 10%$V_2O_5$/γ-$Al_2O_3$ sample exhibited higher initial heat of about 141 kJ mol$^{-1}$, close to that of the γ-$Al_2O_3$ support, indicating the breaking of the polymeric two-dimensional vanadia network, exposing the γ-$Al_2O_3$ surface again to ammonia.

In Fig. 9 are shown the IR spectra collected after exposure of γ-$Al_2O_3$ and $V_2O_5$/γ-$Al_2O_3$ samples to ammonia at room temperature. The bands at 1619 and 1246 cm$^{-1}$ for γ-$Al_2O_3$ belong to the asymmetric and symmetric deformations, respectively, of ammonia coordinated to aluminum cations, representing Lewis acid sites on γ-$Al_2O_3$ [40]. The bands at 1686, 1478 and 1392 cm$^{-1}$ are owing to $NH_4^+$ species formed by the interaction of $NH_3$ with surface Brönsted acid sites. The addition of 3%$V_2O_5$ resulted in the significant decrease of the bands around 1686, 1392 and 1246 cm$^{-1}$, indicating the interaction of added vanadium species with Lewis acid sites of γ-$Al_2O_3$. The addition of $V_2O_5$ also covered the Brönsted acid sites of γ-$Al_2O_3$ since the band for Brönsted sites around 1478 cm$^{-1}$ for γ-$Al_2O_3$ shift to lower frequencies. In fact, the band shifted to 1450 and 1437 cm$^{-1}$, respectively, for the 10 and 25% samples. On the other hand, the band around 1246 cm$^{-1}$ for γ-$Al_2O_3$ shifted to 1259 and 1254 cm$^{-1}$ for the 10%$V_2O_5$/γ-$Al_2O_3$ and 25%$V_2O_5$/γ-$Al_2O_3$ samples, indicating

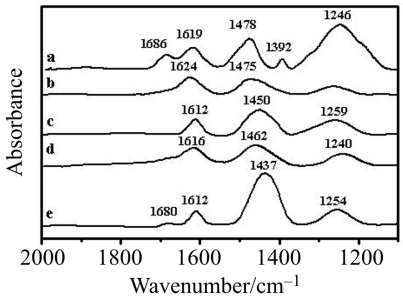


**Fig. 9** FT-IR spectra collected after ammonia adsorption at room temperature on a – γ-$Al_2O_3$, $V_2O_5$/γ-$Al_2O_3$ catalysts with the $V_2O_5$ loading of b – 3%, c – 10%, e – 25% and 10% $V_2O_5$/γ-$Al_2O_3$ treated in $H_2$ d – at 640 K

the Lewis acid sites on vanadium species in the samples. Figure 9e showed that the 25%$V_2O_5$/γ-$Al_2O_3$ sample exhibited mainly Brönsted acid sites on the surface. By comparing the spectra of Fig. 9c and d, it is seen that the reduction of the 10%$V_2O_5$/γ-$Al_2O_3$ sample brought about an increase of frequency of the band for Brönsted acid sites from 1450 to 1462 $cm^{-1}$ and a decrease of frequency of the band for Lewis acid sites from 1259 to 1240 $cm^{-1}$. This clearly reveals the exposure of the surface acid sites associated with γ-$Al_2O_3$ support upon the reduction, consisting with the microcalorimetric adsorption results reported above.

*$V_2O_5$/$TiO_2$*

In Fig. 10 are shown the XRD patterns for $V_2O_5$/$TiO_2$ samples. No crystalline $V_2O_5$ phase was detected for the 3%$V_2O_5$/$TiO_2$, indicating the high dispersion of vanadia species in this sample. Only trace of the crystalline $V_2O_5$ phase can be seen in the XRD pattern for the 10%$V_2O_5$/$TiO_2$. The dispersion of vanadia species in this sample might be still high. The formation of crystalline $V_2O_5$ in the 25%$V_2O_5$/$TiO_2$ sample was apparent according to the XRD spectrum in Fig. 10c. The XRD patterns for $TiO_2$ exhibited typical anatase diffraction peaks.

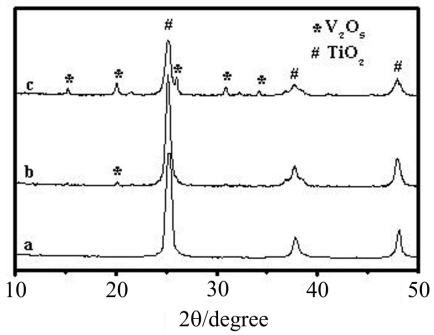


**Fig. 10** X-ray diffraction patterns for $V_2O_5$/$TiO_2$ samples with the $V_2O_5$ loading of a – 3%, b – 10% and c – 25%

Figure 11 shows the DRS spectra for the $V_2O_5$/$TiO_2$ samples with different loadings. The absorption edge energy for the 25%$V_2O_5$/$TiO_2$ sample was almost the same as that for the bulk $V_2O_5$. Since the surface area of the $TiO_2$ support was low as compared to those of γ-$Al_2O_3$ and $SiO_2$, the vanadia phase in the 25%$V_2O_5$/$TiO_2$ sample can be taken as the same as bulk $V_2O_5$. The 3%$V_2O_5$/$TiO_2$ sample exhibited quite high absorption edge energy around 3 eV, indicating the high dispersion of vanadia species in this sample. In addition, it is clearly seen from the DRS spectra that the 10%$V_2O_5$/$TiO_2$ sample exhibited the surface $V_2O_5$ structure that was significantly different from that of bulk. Thus, the structure of vanadia species in the 10%$V_2O_5$/$TiO_2$ sample might be in the form of completed polymeric two-dimensional vanadia network with a little of crystalline $V_2O_5$, while the structure of vanadia species in the 3%$V_2O_5$/$TiO_2$ sample may be taken as the incomplete polymeric two-dimensional vanadia network with some 'holes'. These differ-

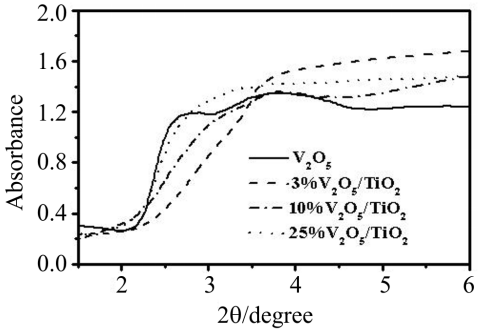


**Fig. 11** DRS spectra for $V_2O_5/TiO_2$ catalysts

ent surface structures of vanadia species for the $V_2O_5/TiO_2$ samples determined their surface acidities.

In Fig. 12 are shown the acidic properties of the $V_2O_5/TiO_2$ samples as measured by microcalorimetric adsorption of ammonia. All the samples were calcined at 673 K before the ammonia adsorption. Figure 12 shows that the $TiO_2$ support exhibited weak acidity with the initial heat of 67 kJ μmol$^{-1}$ and saturation coverage of 65 μmol g$^{-1}$ for $NH_3$ adsorption. The three $V_2O_5/TiO_2$ samples displayed the similar uptakes for ammonia adsorption (about 375 μmol g$^{-1}$), but the initial heats for ammonia adsorption were significantly different. The 3%$V_2O_5/TiO_2$ sample exhibited the highest initial heat of about 137 kJ mol$^{-1}$ while the 10%$V_2O_5/TiO_2$ the lowest of about 89 kJ mol$^{-1}$ for the adsorption of ammonia. The 25%$V_2O_5/TiO_2$ sample displayed the initial heat of about 122 kJ mol$^{-1}$, which was in between those for the 3 and 10% $V_2O_5/TiO_2$ samples. Figure 13 showed that there was no significant difference in nature for the surface acidity for the 3 and 10%$V_2O_5/TiO_2$ samples. Brönsted acid sites dominated the surface acidity for these two samples. The difference might be that the 10%$V_2O_5/TiO_2$ sample possessed a little more Lewis acid sites than the 3% $V_2O_5/TiO_2$ sample as can be seen by comparing the intensities of the bands around

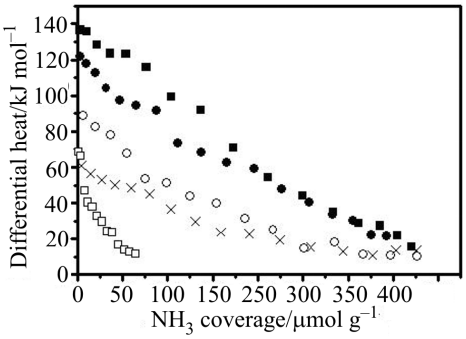


**Fig. 12** Differential heat *vs.* adsorbate coverage for adsorption of $NH_3$ at 150°C on □ – $TiO_2$, ■ – 3% $V_2O_5/TiO_2$, ○ – 10% $V_2O_5/TiO_2$, ● – 25% $V_2O_5/TiO_2$ and 10% $V_2O_5/TiO_2$ treated in $H_2$ at 640 K

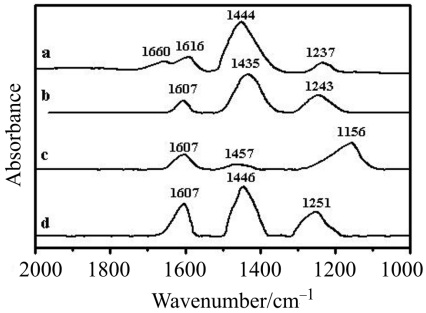


**Fig. 13** FT-IR spectra collected after ammonia adsorption at room temperature on $V_2O_5/TiO_2$ catalysts with the $V_2O_5$ loading of a – 3%, b – 10%, c – 10% $V_2O_5/TiO_2$ treated in $H_2$ at 640 K, d – 25%

1240 cm$^{-1}$ for the spectra of Fig. 13a and b, probably owing to the formation of some crystalline $V_2O_5$ in the 10%$V_2O_5/TiO_2$ sample. The difference in acid strength for the 3 and 10%$V_2O_5/TiO_2$ samples might be due to the different dispersions of surface vanadia species and/or the difference of surface structures. It is suggested that the Brönsted acid site might be Ti–O–V–OH in the 3%$V_2O_5/TiO_2$ sample while V–O–V–OH in the 10%$V_2O_5/TiO_2$ sample. This suggestion is supported by the XRD and DRS results presented above. In this case, the Brönsted acidity of Ti–O–V–OH must be stronger than that of V–O–V–OH. In fact, the acidity of the 3%$V_2O_5/TiO_2$ sample was significantly stronger than that of all supported 25%$V_2O_5$ samples studied in this work.

The 25%$V_2O_5/TiO_2$ sample also exhibited higher acidity than the 10%$V_2O_5/TiO_2$ sample. Figure 13 shows that Lewis acidity was increased significantly in this sample as compared to other $V_2O_5/TiO_2$ samples. This must be a feature of crystalline $V_2O_5$ on the surface of the 25%$V_2O_5/TiO_2$ catalyst. Therefore, the 10%$V_2O_5/TiO_2$ exhibited lower acidity than both the 3%$V_2O_5/TiO_2$ and 25%$V_2O_5/TiO_2$. The vanadia species in the 10%$V_2O_5/TiO_2$ sample might be mainly in the form of completed polymeric two-dimensional network lacking defects (or Ti–O–V–OH groups) and crystalline $V_2O_5$.

The reduction of the 10mass%$V_2O_5/TiO_2$ catalyst in $H_2$ resulted in the significant decrease of the heat for ammonia adsorption, indicating the weakening of the surface acidity upon the reduction. Figure 13 shows that the band at 1435 cm$^{-1}$ for Brönsted acid sites of vanadia and that at 1243 cm$^{-1}$ for Lewis acid sites of vanadia almost disappeared while a new band around 1156 cm$^{-1}$ appeared, representing the Lewis acidity of $TiO_2$ surface. This revealed that the reduction destroyed the polymeric two-dimensional vanadia network on the surface of the 10%$V_2O_5/TiO_2$ sample leading to the exposure of $TiO_2$ surface.

## Conclusions

The dispersion and surface structure of vanadia species strongly depend on the nature of supports and loading and affect the surface acidity. There are mainly three differ-

ent forms of surface vanadia species: (1) isolated tetrahedral species, (2) polymeric two-dimensional network and (3) polycrystalline $V_2O_5$. When $SiO_2$ support is used, the main surface species is the polycrystalline vanadia even for the sample with the loading as low as 3%. The number and strength of acid sites for the $V_2O_5/SiO_2$ samples increase significantly with the increase of vanadia loading. Both Brönsted and Lewis acid sites are present equivalently on the surface of the $V_2O_5/SiO_2$ samples owing to the polycrystalline nature of the surface vanadia species. Vanadia can be well dispersed on $\gamma$-$Al_2O_3$ and $TiO_2$ to form the isolated tetrahedral structure and the polymeric two-dimensional network when the loadings are low. When vanadia is added to $\gamma$-$Al_2O_3$, the Brönsted and Lewis acid sites of $\gamma$-$Al_2O_3$ are covered and the Brönsted and Lewis acid sites of vanadia are formed, leading to the decreased acid strength. In addition, while Lewis sites dominate the surface acidity of $\gamma$-$Al_2O_3$ support, Brönsted sites dominate the surface acidity of $V_2O_5/\gamma$-$Al_2O_3$ catalysts. The surface structure of vanadia in the $3\%V_2O_5/TiO_2$ catalyst can be taken as the incomplete polymeric two-dimensional network and the catalyst may mainly possess the acidic groups Ti–O–V–OH that exhibit strong Brönsted acidity (about 140 kJ $mol^{-1}$ for ammonia adsorption). In contrast, the completed polymeric two-dimensional network formed on the surface of the $10\%V_2O_5/TiO_2$ catalyst may have surface V–O–V–OH groups that show much lower Brönsted acidity (about 90 kJ $mol^{-1}$ for ammonia adsorption). When the loading is high (25%), polycrystalline $V_2O_5$ is the main surface species that display the mediate acid strength (120 kJ $mol^{-1}$ for ammonia adsorption) and possess both Brönsted and Lewis acid sites. The reduction of the supported vanadia catalysts removes the surface V–OH groups, producing Lewis acidity from reduced vanadium species and the surfaces of supports ($\gamma$-$Al_2O_3$ and $TiO_2$).

* * *

This work is supported by the National Natural Science Foundation of China (grant no. 29973013) and the Department of Science and Technology of China (grant no. G199022408). Financial supports from the French Minister of National Education Research is also acknowledged.

## References

1 M. S. Wainwright and N. R. Foster, Catal. Rev. Sci. Eng., 19 (1979) 211.
2 V. Nikolov, D. Kissurski and A. Anastasov, Catal. Rev. Sci. Eng., 33 (1991) 1.
3 F. Cavalli, F. Cavani, I. Manenti and F. Trifirò, Catal. Today, 1 (1987) 245.
4 M. Sanati and A. Anderson, J. Mol. Catal., 59 (1990) 233.
5 H. Bosch and F. Janssen, Catal. Today, 2 (1988) 369.
6 J. Svachula, L. J. Alemany, N. Feriazzo, P. Forzatti, E. Tronconi and F. Bregani, Ind. Eng. Chem. Res., 32 (1993) 826.
7 W. I. Prins and Z. L. Numinga, Catal. Today, 16 (1993) 187.
8 E. A. Mamedov and V. C. Corberan, Appl. Catal. A, 127 (1995) 1; and H. H. Kung, Adv. Catal., 40 (1994) 1.
9 W. Harding, K. R. Birkel and H. H. Kung, Catal. Lett., 28 (1994) 1; and L. Owens and H. H. Kung, J. Catal., 148 (1994) 587.

10 A. Ramsetter and M. Baerns, J. Catal., 109 (1988) 303.
11 N. T. Do and M. Baerns, Appl. Catal., 45 (1988) 1.
12 P. M. Michalakos, K. Birkeland and H. H. Kung, J. Catal., 158 (1996) 349.
13 G. Deo and I. E. Wachs, J. Catal., 146 (1994) 323.
14 P. Forzatti, E. Tronconi, G. Busca and P. Tittarelli, Catal. Today, 1 (1987) 2089.
15 G. C. Bond and S. F. Tahir, Appl. Catal., 71 (1991) 1.
16 G. T. Went, S. T. Oyama and A. T. Bell, J. Phys. Chem., 94 (1990) 4240.
17 I. E. Wachs, R. Y. Saleh, S. S. Chan and C. C. Chersich, Appl. Catal., 15 (1985) 339.
18 J. Haber, A. Kozlowska and R. Kozlowski, J. Catal., 102 (1986) 52.
19 F. Arena, N. Giordano and A. Parmaliana, J. Catal., 166 (1997) 66.
20 S. T. Oyama, G. T. Went, K. B. Lewis, A. T. Bell and G. A. Somorjai, J. Phys. Chem., 93 (1989) 6786.
21 M. M. Kantcheva, L. I. Hadjiivanov and D. G. Klissurski, J. Catal., 134 (1992) 299.
22 T. Kataoka and J. A. Dumesic, J. Catal., 112 (1988) 66.
23 I. E. Wachs, Catal. Today, 27 (1996) 437.
24 A. M. Turek and I. E. Wachs, J. Phys. Chem., 96 (1992) 5000.
25 G. Busca, F. Ramis and V. Lorenzelli, J. Mol. Catal., 50 (1989) 231.
26 J. Datka, A. M. Turek, J. M. Jehng and I. E. Wachs, J. Catal., 135 (1992) 186.
27 H. Miyata, K. Fuji and T. Ono, J. Chem. Soc., Faraday Trans., 84 (1988) 3121.
28 J. Shen, R. D. Cortright, Y. Chen and J. A. Dumesic, J. Phys. Chem., 98 (1994) 8067.
29 A. Khodakov, B. Olthof, A. T. Bell and E. Iglesia, J. Catal., 181 (1999) 205.
30 J. Tauc, in Amorphous and Liquid Semiconductors, Tauc, J., Ed., Plenum Press, London 1974, p. 171.
31 R. S. Weber, J. Catal., 151 (1995) 470.
32 E. Iglesia, D. G. Barton, S. L. Soled, S. Miseo, J. E. Baumgartner, W. E. Gates, G. A. Fuentes and G. D. Meitznerm, Stud. Surf. Sci. Catal., 101 (1996) 533.
33 A. Khodakov, J. Yang, S. Su, E. Iglesia and A. T. Bell, J. Catal., 177 (1998) 343.
34 A. P. Alivasatos, Science, 271 (1996) 933.
35 R. F. Service, Science, 271 (1996) 920.
36 M. L. Good, Spectrochim. Acta A, 29 (1973) 707.
37 H. So and M. T. Pope, Inorg. Chem., 11 (1972) 1441.
38 M. Iwamoto, H. Furukawa, K. Matsukami, T. Takenaka and S. Kagawa, J. Am. Chem. Soc., 105 (1983) 3719.
39 H. Ronde and J. G. Snijders, Chem. Phys. Lett., 50 (1977) 282.
40 J. Shen, R. D. Cortright, Y. Chen and J. A. Dumesic, Catal. Lett., 26 (1994) 247.